



Research Article

Theme: Advancements in Amorphous Solid Dispersions to Improve Bioavailability

The Physical Stability of Felodipine and Its Recrystallization from an Amorphous Solid Dispersion Studied by NMR Relaxometry

A. Pajzderska,^{1,4}  J. Mielcarek,² and J. Wąsicki^{1,3}

Received 30 November 2021; accepted 9 February 2022; published online 21 March 2022

Abstract. The ¹H nuclear magnetic resonance (NMR) relaxometry method was applied to investigate the physical stability of an active pharmaceutical ingredient (API) and, for the first time, its recrystallization process in an amorphous solid dispersion system (ASD). The ASD of felodipine and polyvinylpyrrolidone (PVP) was prepared using the solvent evaporation method in a mass ratio of 50:50. In the first stage of the study (250 days), the sample was stored at 0% relative humidity (RH). The recovery of magnetization was described by one-exponential function. In the second stage (300 days in 75% relative humidity), the recrystallization process of felodipine was studied, showing in the sample three components of equilibrium magnetization related to (i) crystalline felodipine, (ii) water, and (iii) felodipine and PVP remaining in the ASD. The study shows that the ¹H NMR relaxometry method is a very useful tool for analysing the composition of a three-phase system mixed at the molecular level and for the investigation of recrystallization process of API in amorphous solid dispersion system.

KEY WORDS: physical stability; recrystallization; relaxometry; amorphous solid dispersion; felodipine; PVP; time-domain NMR.

INTRODUCTION

The most new active pharmaceutical ingredients (APIs) and those synthesized in recent years are characterized by poor aqueous solubility (1–3) and at least 40% of active compounds belong to the Biopharmaceutics Classification System (BCS) class II (4, 5). This low solubility is associated with insufficient oral bioavailability and therefore is now one of the main challenges in drug development, especially in its solid oral dosage forms in the pharmaceutical industry (6, 7). Generally, amorphization of an API increases its solubility and thus bioavailability. However, the amorphous form has lower physical stability compared to the more stable crystalline form. One way to improve the stability of the amorphous state is to mix a hydrophobic API with a hydrophilic polymer. For maximum physical stability, mixing should be done at the molecular level and such a formulation is called an

amorphous solid dispersion (ASD), where drug and polymer are intimately mixed (1, 8). Such a sample is homogeneous on the spatial scale (drug and polymer domains have average dimensions smaller than 100 Å). Formulating an API as an amorphous solid dispersion has been proven to successfully enhance aqueous solubility and bioavailability of many APIs (6, 9, 10). So, it is most often the case that amorphous forms of API in ASD are much more stable than in the pure state, but the stability of such a system is also influenced by many other factors. These are internal factors (type of API and polymer and their proportions) and external factors, mainly temperature and humidity (1, 8, 11).

Many literature reports emphasize the great importance of water for the physical stability of ASD. Among other things, it is noted that the water present in ASD lowers its T_g (12). In addition, it changes the composition of the system, becoming its third component, and thanks to its mobility, it increases the mobility of the entire formulation, which greatly facilitates API recrystallization. Thus, API recrystallization is one of the most frequently observed manifestations of ASD's physical instability and influence on limited marketed formulations. Therefore, API crystallization in ASDs should be considered as a potential risk to both patients and pharmaceutical companies and the methods which allow the possible recrystallization process to be followed are necessary (13).

Rumondor *et al.* (14) observed two possible routes of drug recrystallization in an amorphous solid dispersion

¹ Department of Medical Physics and Radiospectroscopy, Faculty of Physics, Adam Mickiewicz University, Uniwersytetu Poznańskiego 2, 61-614, Poznan, Poland.

² Department of Inorganics and Analytical Chemistry, Poznań University of Medical Sciences, Grunwaldzka 6, 60-780, Poznan, Poland.

³ NanoBioMedical Centre, Adam Mickiewicz University, Wszechnicy Piastowskiej 3, 61-614, Poznan, Poland.

⁴ To whom correspondence should be addressed. (e-mail: apajzder@amu.edu.pl)

system (containing a hydrophobic drug and a hydrophilic polymer) under conditions of increased humidity. One possibility is crystallization from a plasticized single-phase solid dispersion, and the other is crystallization from a plasticized drug-rich amorphous phase in a two-phase solid dispersion. In the first case, the polymer is in the same phase as the drug, so the system should consist of three components: the crystalline drug, polymer/drug, and water. In the second case, the polymer content in the drug phase decreases due to separation of the amorphous and amorphous phases, and the system should consist of four components: the crystalline drug, amorphous drug, polymer, and water.

The following methods are used to study the properties of ASD: differential scanning calorimetry (DSC) (15), powder X-ray diffraction (PXRD) (16, 17), optical spectroscopy (16, 17), and dielectric spectroscopy (18). Among these, solid-state nuclear magnetic resonance (ssNMR), which is a non-destructive potent technique, plays an essential role in the description of materials (19–23) because it can provide information about molecular miscibility (24), molecular mobility and motions (19, 23, 25, 26), and intra- and intermolecular drug interactions with polymers in ASD at an atomic level (21–23). In particular, the ssNMR method is used to qualitatively differentiate and to quantify such components in complex formulations as polymorphs of APIs, their crystalline and amorphous forms or excipients (23). Both high-resolution NMR and low-field NMR could be also used to investigation the degree of mixing between drug and polymer (27, 28). Especially, time-domain NMR (TD-NMR) in which spin-lattice T_1 and spin-spin T_2 relaxation times are measured at low-field is applied in the pharmaceutical field. As TD-NMR spectrometers are usually a benchtop instruments, the relaxometry measurements can be rapidly and easily (29, 30).

The DSC (31, 32) and PXRD (33–35) methods are increasingly used to study the recrystallization process of pure API. Other methods are optical microscopy (36–39), transmission electron microscopy (TEM) (40), Raman spectroscopy (35, 41), dielectric spectroscopy (42) and terahertz spectroscopy (43), and NMR relaxometry (44). NMR relaxometry was also used to study the API recrystallization process in an API-polymer physical mixture, where drug and polymer are not intimately (approximately on a 100-Å scale) mixed and two distinct types of submillimeter size grains exist (45). The recrystallization of API in the ASD system is a more complex process, which was studied, for example, for felodipine and polymers — polyvinylpyrrolidone (PVP) and hypromellose acetate succinate (HPMCAS) by means of the PXRD method (46). Moreover, the time-domain (TD) NMR method (47) was applied to ASD systems (carbamazepine/polyvinylpyrrolidone (hereafter PVP) and indomethacin/PVP) and a modification of the magnetization recovery due to partial recrystallization of APIs in ASD was noticed (29). However, in this work, there was no quantification of the observed API recrystallization.

The aim of the present study is to investigate the physical stability of amorphous API and its recrystallization in ASD by NMR relaxometry. In the first stage of the study, ASD was stored in 0% relative humidity (RH), i.e., it was examined whether recrystallization could occur in such condition and to get suggestion about achievable shelf life. In the second part, the sample was under environmental stress, i.e., was stored in

75% RH. Felodipine with PVP was selected for this research. Felodipine belongs to a class of drugs called calcium channel blockers from the group dihydropyridine derivatives. It relaxes the blood vessels and is used to treat high blood pressure. Felodipine in its crystalline and amorphous form and in a mixture with polymers is widely studied by numerous scientific teams and can therefore be treated as a model compound (31, 35–37, 39, 44–57). On the other hand, PVP (with a varying chain length and molecular weight) is a very common polymer in ASD (58). NMR relaxometry has already been used successfully to evaluate the recrystallization of amorphous felodipine (44) and for the recrystallization of amorphous felodipine in a mixture with PVP (45). In the first case, except for the initial and final state, the system was two-phase (components related to amorphous and crystalline felodipine). In the second case, the system, except for the initial and final states, was three-phase; components related to amorphous crystalline felodipine and PVP have been observed. The choice of felodipine/PVP system for our research will enable the comparison of the results with the recrystallization process studied by PXRD (46). Additionally, our study will indicate the recrystallization route in our ASD sample. To the best of our knowledge, this method (NMR relaxometry) was used to quantify the recrystallization process in ASD for the first time.

MATERIALS AND METHODS

Sample Preparation and Characterizations

Amorphous Solid Dispersion. Felodipine ($C_{18}H_{19}Cl_2NO_4$) and the polyvinylpyrrolidone (PVP, average molecular weight 10 kg/mol, $(C_6H_9NO)_n$) were purchased from TCI, Japan, and Sigma-Aldrich, respectively. Felodipine (form 1) was previously described by means of the differential scanning calorimetry (DSC), powder X-ray diffraction (PXRD), and Fourier transform infrared spectroscopy (FTIR) methods (48). The amorphous solid dispersion sample was prepared using the solvent evaporation method: 0.5 g of felodipine, which had previously been dried for 24 h at 110°C, was weighed into a 500-ml round-bottom flask, and 100 ml of anhydrous ethanol was added. Then, 0.5 g of polyvinylpyrrolidone was dissolved in 100 ml of dichloromethane and added dropwise to the flask. The flask was sealed, and the solution was stirred for 24 h at 25°C and 400 rpm. The solvent was then removed on a Rotavapor R-100 Buchi rotary evaporator. The resulting material was crushed and dried under reduced pressure for 24 h to remove any residual solvents. The material was again triturated and dried for 10 h at 25°C in a Glass Oven B-585 Buchi.

Preliminary Characterization of the Sample. Powder X-ray diffraction measurements were performed just after preparing the system. No diffraction peaks were observed, only a broad amorphous halo with two maxima at 11 and 22° (Fig. S1). DSC measurements were also performed in the temperature range from 26 to 166°C. Only one anomaly was observed in the DSC curve at 70°C, which is related to the glass transition of ASD. The glass transition temperature T_g is 126°C and 46°C for the PVP studied and amorphous felodipine, respectively. From the Gordon-Taylor (59) equation, the temperature of the glass transition T_g for an ideal

binary mixture was determined and was 67°C, which is very close to the measured one. The single glass transition and the absence of the endothermic peak related to the melting of felodipine indicate a high degree of mixing felodipine with the polymer, i.e., a high degree of homogeneity of the prepared ASD system.

NMR Relaxometry Measurements. The spin-lattice T_1 and spin-spin T_2 relaxation times were measured as a function of the time since preparation of the ASD sample approximately every week. The research was divided into two stages. The first one lasted 250 days, in which the sample was stored at 27°C and 0% RH. The sample was then put through sieves so that the grain sizes were in the range from 0.1 to 0.2 mm and was placed in a desiccator at 75% RH. The material obtained was divided into two parts. T_1 and T_2 relaxation times were then measured approximately every week for the first sample, and for the second sample, PXRD spectra were recorded several times. The second stage of the research lasted 300 days.

Methods

DSC analyses were performed using a PerkinElmer DSC8500 calorimeter. n-Dodecane and indium standards were used for instrument calibration. Heating thermograms were carried out at a standard rate of 10 K/min under a dry nitrogen atmosphere (flow rate 20 ml/min).

Powder X-ray diffraction (PXRD) studies were carried out on powdered samples using a Bruker D8 Advance diffractometer with Cu K α radiation ($\lambda = 1.54 \text{ \AA}$) and a LynxEye detector, operating in Bragg-Brentano geometry. Scans were recorded at room temperature (300 K) in angles ranging from 5 to 50 ($^{\circ}2\theta$) with a step size of 0.03 and continuous scan mode.

^1H NMR Measurements. The samples for the ^1H NMR measurements were placed in a glass ampoule with an inner diameter of 8 mm. All measurements were performed using a relaxometer working at a resonant frequency of 25.0 MHz (EI-Lab Tel-atomic). A saturation pulse sequence (25 pulses 90°_x of 4.2 μs separated by 4.2 μs) and, after time τ , probing pulses were applied. As probing pulses, the “solid echo” (60, 61) sequence $90^{\circ}_y\text{-}\tau\text{-}90^{\circ}_x$ was used, which has the advantage that FIDs are not distorted by the dead time of the radio frequency pulse. FIDs were recorded for 64 time intervals τ (ranging from 5 ms to 50 s) between the saturation series and the probing pulse. To improve the signal-to-noise ratio (S/N), four accumulations were used. All measurements were made at 295 K.

The FID curves (detected for maximum τ) were fitted by the linear combination of two functions (Gaussian and exponential function):

$$A(t) = A_0^G \exp\left(-\left(t/T_2^G\right)^2\right) + A_0^E \exp\left(-t/T_1^E\right) \quad (1)$$

where A denotes the amplitude of given component, and T_2 the spin-spin relaxation time; the superscript “G” denotes the

Gaussian function, while superscript “E” denotes the exponential component characterized by a longer relaxation time.

The spin-lattice relaxation time T_1 was extracted from the saturation recovery curve (magnetization recovery) obtained from the evolution of FID in a function of τ . The magnetization recovery curve for multiphase systems can be described with the following expression:

$$M_z = \sum_{i=1}^N M_0^i (1 - \exp(-t/T_1^i)) \quad (2)$$

where N denotes the maximum number of phases, T_1^i are the values of relaxation time in a given phase, and M_0^i are the contributions to the total magnetization arising from these phases 1, 2, and 3. The fraction of each of the phases can then be calculated from the following formula:

$$fr_i = \frac{M_0^i}{\sum_{i=1}^N M_0^i} \quad (3)$$

The experimental curves were fitted using the least-squares method or non-linear least-squares fitting using the Levenberg-Marquardt algorithm in the PeakFit program (62).

The quality of the magnetization recovery curves depends on the number of accumulations and the mass of the sample (in our case these were 4 and approx. 0.4 g, respectively). Such measurement parameters allow to properly distinguish the phases and determine the fraction of each phase with an accuracy of 3–5% if the relaxation times T_1 of selected components differ at least about 20–30%.

RESULTS

The Physical Stability of Felodipine in ASD — Spin-Lattice T_1 and Spin-Spin T_2 Relaxation Times in the First Stage of the Study (0% RH)

The relaxation time T_1 as a function of time since sample preparation is shown in Figure 1. The value of the time T_1 immediately after sample preparation was 800 ms. This is an intermediate value between the T_1 for PVP (80 ms) (45) for amorphous felodipine (1500 ms) (44, 45). It is worth underlining that all recoveries of magnetization curves were one-exponential and fitted by Formula (2), assuming $N = 1$. Such magnetization behavior confirms the homogeneity of the system in which spin-lattice relaxation times are the average of the single value throughout the sample, due to the spin diffusion (19, 63). Interestingly, the value of T_1 after the first decay was approximately constant up to 70 days and then decreased monotonically in a function of time to 300 ms on day 250.

Figure 2 shows the shape of FID recorded 250 days after sample preparation. The analysis of FID decay provides information about regions of the sample with possible different mobilities. This curve is described by means of two

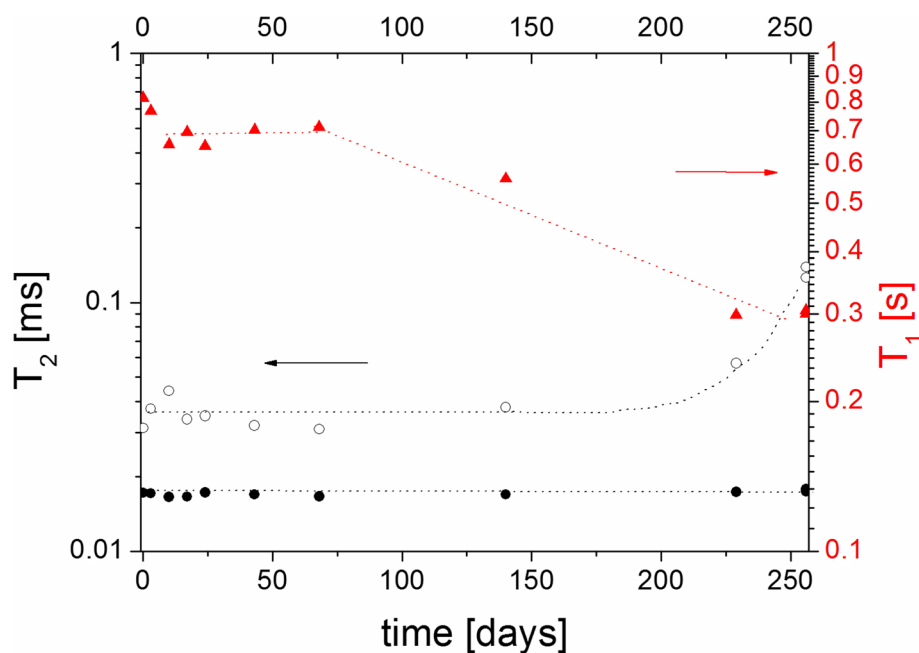


Fig 1 Spin-lattice T_1 (filled triangle) and spin-spin T_2 relaxation times (open circle, long component, filled circle short component) in a function of time since the ASD sample preparation (first stage of the study). The dot lines are guided by eyes

functions, Gaussian and exponential (Eq. (1)), and each function is related to one of the motionally distinguishable regions. The value determined for the spin-spin T_2^G relaxation time for the component described by the Gaussian function was $\sim 17 \mu\text{s}$ and did not change with time. On the other hand, the T_2^L constant up to 140 days from the

sample preparation and equal to $\sim 32 \mu\text{s}$ and then T_2^L increased and reached a value of $\sim 126 \mu\text{s}$ on day 250 (Fig. 1). The amplitudes of the given components were constant over time and stood at 0.83 and 0.17 for A_0^G and A_0^L , respectively, which means that the number of protons belonging to these components remains constant. As the

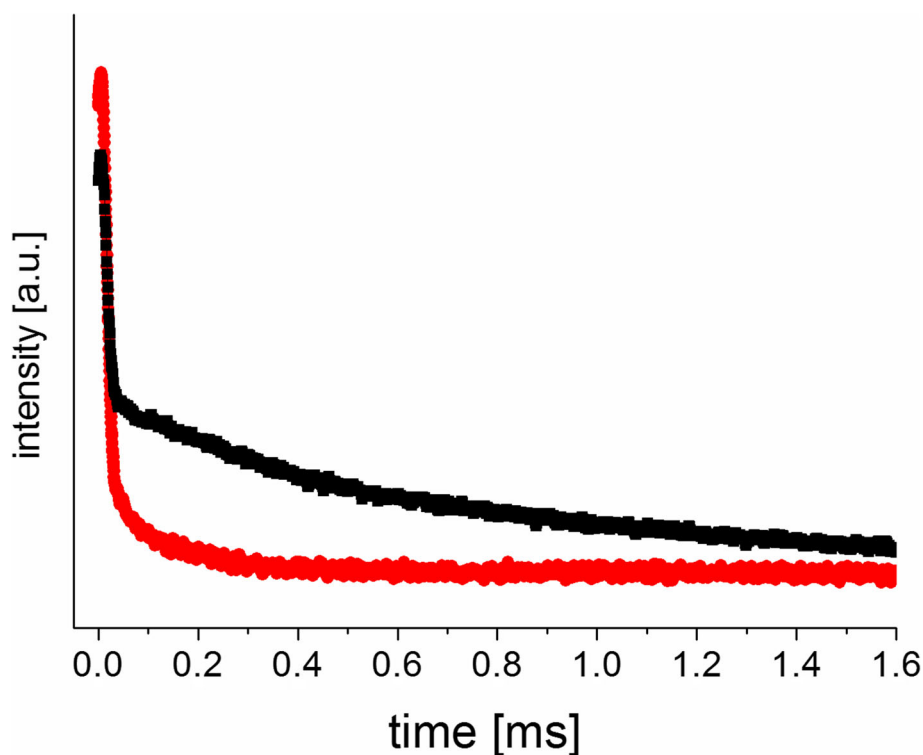


Fig. 2 FID curves measured for ASD (filled red circle) first stage of the study (0% RH), (filled black square) second stage of the study (75% RH)

relaxation times T_2 are relatively short, both components correspond to the solid phase, although the T_2^L of the component described by the exponential function indicates the presence of a small, more mobile part in the system.

In order to quantify the domain sizes in the ASD sample, measurements of the T_1 spin-lattice relaxation time should be analyzed. Based on these data, the maximum size of the L domains can be estimated from the following formula (64–66):

$$L = \sqrt{6DT_1} \quad (4)$$

where D is the spin diffusion coefficient.

The diffusion coefficient D (Eq. (4)) depends on the distance between protons r_{HH} in the system and on the dipolar coupling, which is proportional to the line width of the ^1H signal $\Delta\nu_{1/2}$ (66). As line width is proportional to the spin-spin relaxation time T_2 , the diffusion coefficient can be described as follows:

$$D \sim \Delta\nu_{1/2}(r_{\text{HH}})^2 \sim (1/\gamma)(1/T_2)(r_{\text{HH}})^2 \quad (5)$$

where γ is gyromagnetic ratio.

As experimentally T_2^G does not depend on time, the diffusion coefficient D in the system does not change. Assuming a D value of $8 \times 10^{-12} \text{ cm}^2/\text{s}$, which is typical for organic solids (including polymers) (65), it was established that the size of the domains did not exceed 62 nm (just after preparation) and decreased to 37 nm on day 250 after preparation. For a similar system, the estimated minimum value of L domain sizes based on spin-lattice relaxation time measurements in the rotating frame $T_{1\rho}$ was 4–5 nm (56). We can therefore conclude that the ageing of the ASD sample at zero humidity does not cause felodipine recrystallization and results obtained suggests that domain sizes decreases. Our studies also indicate that the shelf life of an ASD sample stored in 0% RH is at least 6 months.

The Recrystallization of Felodipine — Spin-Lattice T_1 and Spin-Spin T_2 Relaxation Times in the Second Stage of the Study (75% RH)

During the first 2 days after the sample was placed in 75% humidity, the magnetization recovery was still one-exponential, but after 8 days, the curves became clearly non-exponential. This means that drastic changes occurred, and the system became heterogeneous. This recovery of the magnetization was best described by means of three relaxation processes (Eq. (2), for $N = 3$), which were characterized by the following T_1 time values: 21 ms, 156 ms, and 5700 ms hereinafter referred to as the short, intermediate, and long components, respectively. Figure 3 shows an exemplary fit after 70 days in 75% RH, and Figure S2 shows fits for measurements performed after 30, 70, and 130 days. The T_1 time values (Fig. 4) for the short and intermediate components grow monotonically with time, and their values at the end of measurements (300 days) were 66 ms and 309 ms, respectively. The long component of T_1 time does not change within the limit of measurement accuracy.

As mentioned above, the non-exponential recovery of the magnetization indicated that the sample studied became heterogeneous. The most expected modification to this system is recrystallization of felodipine. This assumption is confirmed by the fact that the value of the long time component T_1 corresponds precisely to the crystalline felodipine. This conclusion is also supported by PXRD measurements. After 30 and 70 days, the PXRD spectra of the ASD sample were also measured. Well-formed Bragg peaks corresponding to crystalline felodipine and halo with maxima for 11 and 22° angles related to the amorphous part of the system were detected (Fig. S1).

The assignment of two other components of the T_1 relaxation times will be based on the analysis of the behavior of their fraction over time (Eq. (3), $N = 3$) in the magnetization (Fig. 5). The fraction of the short component increases monotonically with time, while the fraction of the intermediate component decreases monotonically. However, the fraction of the long component T_1 behaves quite differently, as it grew for up to 50 days, after which it had a constant value of 0.2. Since the fraction of the short component of T_1 time increases with the time that the sample remains at 75% humidity, it should be attributed to the water built in the system (the analysis of the shape of the FID signal presented later in the paper also shows that water is embedded in the sample). The intermediate component of T_1 time can be ascribed to that part of the felodipine and PVP in ASD that remained after the partial recrystallization of felodipine. This component can also be related to bound water, free amorphous felodipine, and free PVP. However, all these parts are described by one relaxation time, i.e., spin diffusion averages T_1 between them. T_1 relaxation time of slow and intermediate components increases slightly in a function of time, which means that the mobility of unbounded water is changing. The water that builds into the sample also impacts on the dynamics of remaining PVP and felodipine in ASD.

As was previously shown, the T_1 relaxometry method is suitable for determining the recrystallization process in an amorphous system (44) and in a mixture of amorphous API with PVP (35). Quantitative information on the degree of crystallinity is provided by the analysis of the fraction of magnetization of a given component in the equilibrium magnetization of the sample. If we want to determine the fraction of crystalline felodipine from the measurements of T_1 , we must take into account only the contributions of the long and intermediate T_1 components to the magnetization. The contribution of a component with a short T_1 value should be omitted, because protons from water molecules that build into the system increase the value of the equilibrium magnetization. In addition, such an approach enables the comparison of the results obtained by T_1 relaxometry with those obtained by the PXRD method, because water is not visible in these spectra.

For this reason, the fraction of crystalline felodipine was calculated omitting the contribution to the equilibrium magnetization of the short-time component T_1 (Eq. (3), $N = 2$), and the dependence obtained is shown in Figure 6. This figure also shows the results of recrystallization of felodipine in ASD with PVP over time, as obtained by the PXRD method (36). These results are in good agreement with those obtained using NMR relaxometry.

The fraction of the crystalline phase grows with time, but the increase is faster until the point 200 days from placing the sample in a humidity of 75%. However, even on the last day of measurement, the fraction of crystalline felodipine is

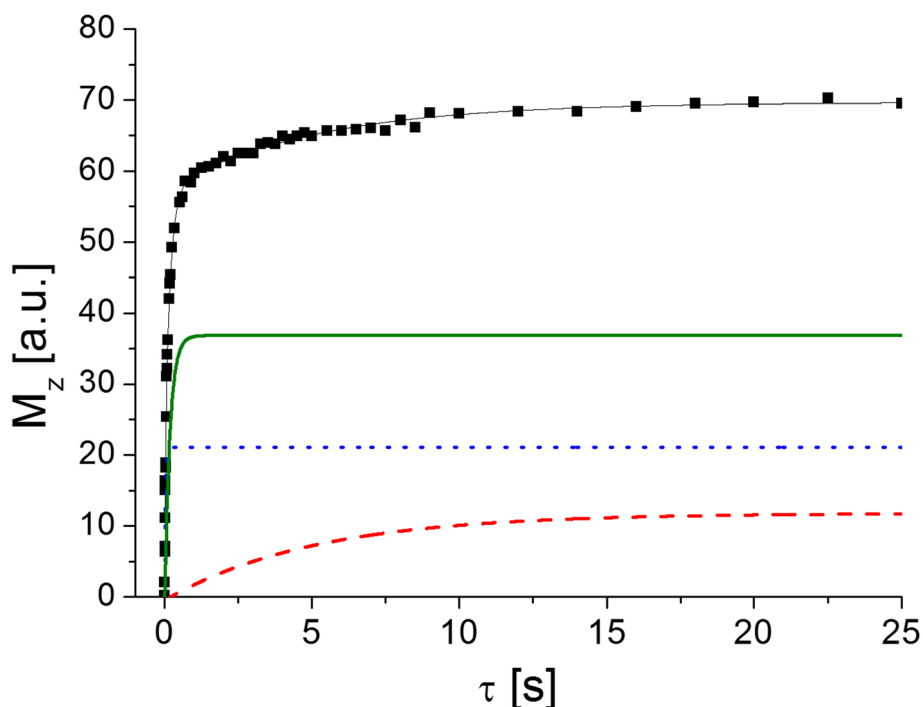


Fig. 3 Magnetization M_z (points) versus time (τ) distance between the saturating series and probing pulse recorded for the ASD sample after 70 days in 75% RH. The lines are the best fit (using Eq. (2), $N = 3$) to the experimental points. The magnetization related to crystalline felodipine — red, dashed line, water — blue, dotted line, to the remaining PVP and felodipine in ASD — green line, the resultant magnetization — black, solid lines

~50%, which means that the remaining 50% is amorphous felodipine hydrogen-bonded with PVP. It should be remembered that the method of preparing ASD we used was the

same as in the paper by Konno *et al.* (50) with the exception of the molecular weight of the PVP (the length of PVP chain) being different.

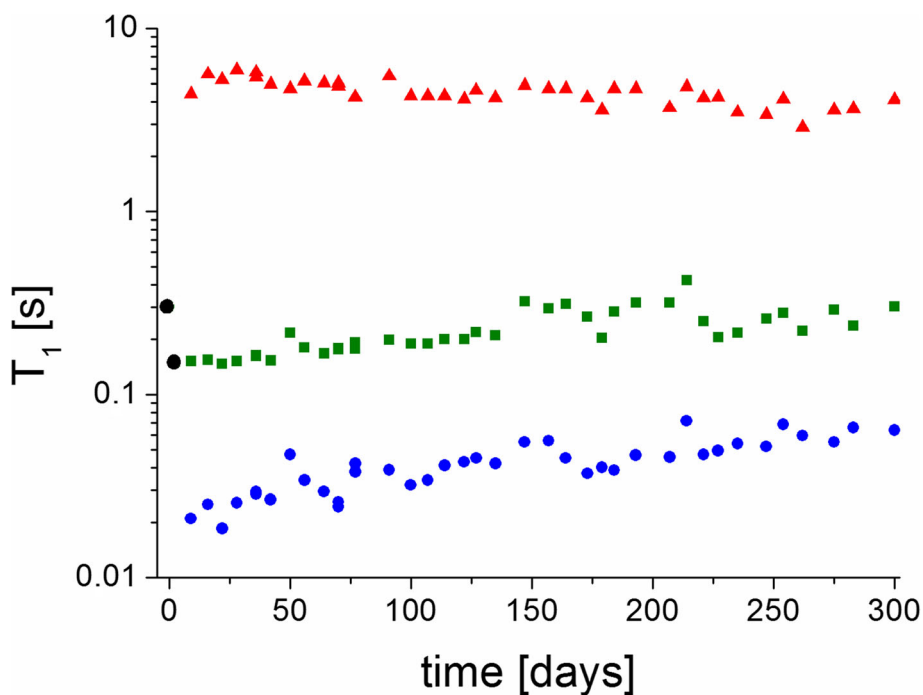


Fig. 4 Dependence of T_1 relaxation times as a function of the time since the ASD sample was placed in 75% humidity, (filled blue circle) component corresponding to water, (filled green square) component corresponding to the remaining PVP and felodipine in ASD, (filled red triangle) component corresponding to crystalline felodipine. T_1 (filled black circle) extracted from one-exponential recovery curves

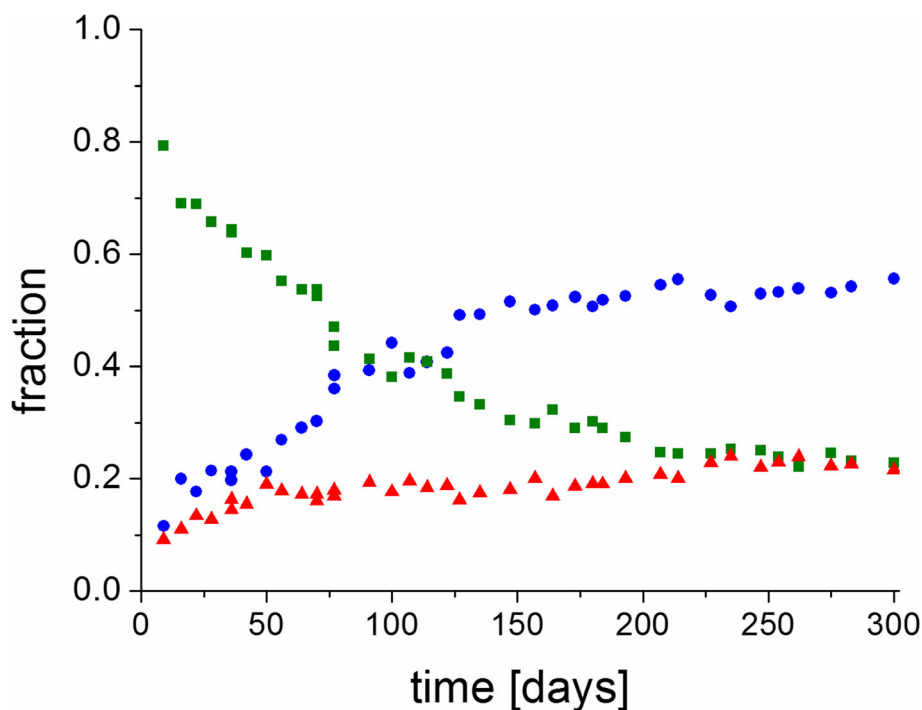


Fig. 5 Dependence of fraction of the magnetization (calculated from Eq. (3)) as a function of the time since the ASD sample was placed in 75% humidity, (filled blue circle) component corresponding to water, (filled green square) component corresponding to the remaining PVP and felodipine in ASD, (filled red triangle) component corresponding to crystalline felodipine

Figure 2 also shows the FID curve recorded after 70 days in a relative humidity of 75%. As in the first stage of the research, this signal was described using two functions, Gaussian and exponential (Eq. (1)), and again, each function corresponds to one of the motionally distinguishable regions. The value of the spin-spin T_2^G relaxation time for the component described by the Gaussian function was $\sim 17 \mu\text{s}$ and did not change with time. This value is very close to that measured for the Gaussian component in the first stage. On the other hand, the value of the spin-spin T_2^L relaxation time for the component described by the exponential function is constant and amounts to approximately 1 ms.

The analysis of FIDs shows that for the ASD sample in 0% and 75% RH, we observe the coexistence of the rigid part characteristic for a solid, which is described by the short time T_2^G , with the mobile part, described by the longer time T_2^L . However, in the sample stored at 0% RH, the fraction of the rigid part in the FID is definitely higher than the fraction of the mobile part. On the other hand, the fractions of the rigid and mobile components in the sample stored at 75% RH are comparable (after 2-3 days from putting the sample to 75% RH).

The T_2^G time values are very similar for the sample stored in 0% and then in 75% RH and do not depend on the time since the sample was prepared. On the other hand, the T_2^L time values for the mobile part are significantly different. The T_2^L time values measured in the first stage of the study are only in the order of tens of μs , which suggests that they are also connected with the solid part of the system, while the T_2^L times in the second stage of the study are of the order of milliseconds and this component corresponds to absorbed water and does not depend on time. Amplitudes A_0^G and A_0^L are similar, which means that the number of protons in the solid part and in the semi-liquid is comparable.

Using the Raman mapping method, Luebbert *et al.* (54) showed that for a wide range of felodipine content in PVP and high humidity, moisture-induced amorphous-amorphous phase separation (APS) was observed. Using the methods of atomic force microscopy, nanothermal analysis, and photothermal infrared microspectroscopy, the authors of the study (67) demonstrated the occurrence of phase separation in a thin film, felodipine-PVP K29/32 under high humidity. PVP cannot prevent phase separation of felodipine under high humidity but can minimize the crystallization of amorphous felodipine domains in the solid dispersion thin films.

The behavior of the sample stored at 75% humidity is definitely different to that in the studies discussed above, in which it was shown that felodipine recrystallization was preceded by APS. In this case, shortly after placing the ASD sample in a humidity of 75%, we should observe the three components of magnetization: from amorphous felodipine, PVP, and water. Over time, a fourth component of the magnetization related to the crystalline felodipine should appear. However, we observe only three components of magnetization assigned to crystalline felodipine, PVP with felodipine, and water. The lack of a component related to amorphous felodipine, for which the T_1 relaxation time is about 1.5 s, indicates that in the ASD studied here, crystallization of felodipine is not prior by APS.

In the ASD samples (felodipine/PVP) in which amorphous-amorphous phase separation was prepared by various methods: solvent evaporation (46, 50, 54), spray drying (50), or a solvent thin film spin-coated onto glass slides (50) and a high molecular weight, a PVP polymer was always used, most often K29/32 and less frequently K25. We prepared the ASD using the solvent evaporation method, similar to the

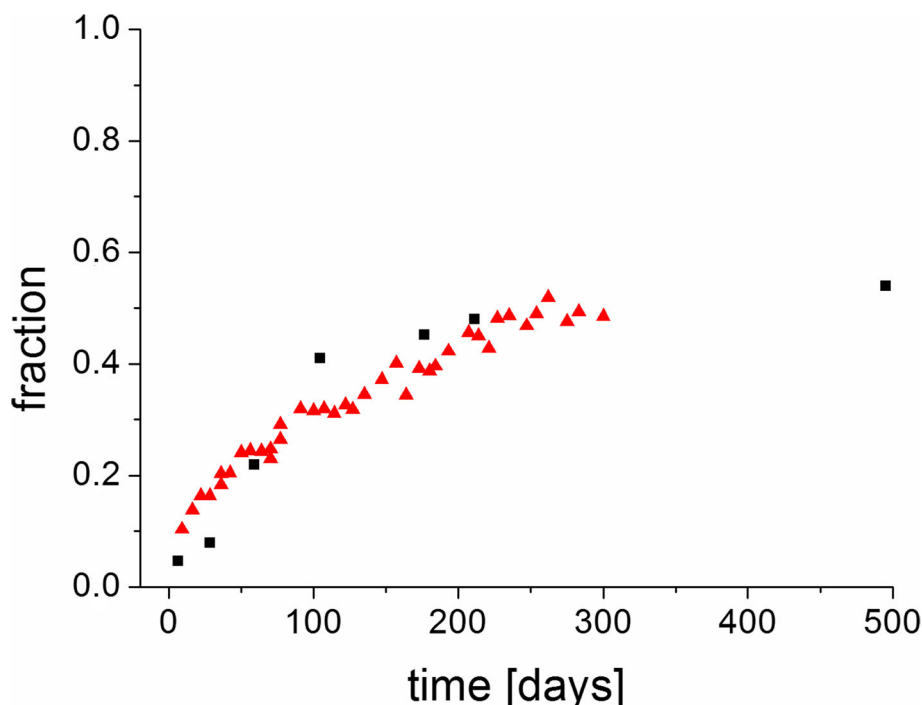


Fig. 6 Dependence of the fraction (filled red triangle) of crystalline felodipine (calculated from Eq. (3) taking into account the component corresponding to crystalline felodipine and the remaining PVP and felodipine in ASD) as a function of the time since the ASD sample was placed in 75% humidity. The fraction (filled black square) of crystalline felodipine from ref. (32) was obtained using the PXRD method

procedure described in the paper (46). However, unlike other authors, we seasoned the sample within 250 days in 0% RH and we used PVP with a lower molecular weight of 10 kg/mol. It seems that this is the most likely reason for such different behavior under the influence of high humidity of our sample compared to the behavior described by other authors. The influence of the molecular weight of the polymer on the degree of mixing of API/PVP components was investigated in the NMR study (52) by measuring the spin-lattice relaxation time in a rotating coordinate system $T_{1\rho}$ for protons. The study was performed for ASD (felodipine/PVP) with 90% by weight of API and for three PVP samples with different weights: K12 (2–3 kg/mol), K25 (28–34 kg/mol), and K90 (1000–1500 kg/mol). It was found that the homogeneity of the mixture was worse for PVP with higher molecular weights, and the reason for this was their lower mobility. Thus, the higher mobility of the lower molecular weight PVP used and increased homogeneity as a result of seasoning in 0% RH may be the reason why felodipine recrystallization was not preceded by the occurrence of APS.

CONCLUSIONS

The sample of amorphous felodipine/PVP solid dispersion was studied by the NMR relaxometry method (T_1 , T_2) and led to the following conclusions:

1. The ageing of the ASD system stored at zero humidity was manifested by a decrease in the domain size of a significant part of the sample (over 80%) and an increase in the mobility of the other area. Felodipine remained amorphous for at least 6 months.

2. The T_1 relaxometry method allowed the process of felodipine recrystallization in ASD stored in 75% humidity to be studied. The results obtained are in strong agreement with those obtained for a similar system using the PXRD method (37).
3. The process of felodipine recrystallization in this system was not preceded by phase separation (APS).
4. The study shows that NMR relaxometry (TD NMR) is a useful and convenient tool for studying the physical stability of API and its recrystallization in an amorphous solid dispersion system, where API is intimately mixed with a polymer at the molecular level. Time domain NMR can be applied in the field of pharmaceutical science not only in scientific laboratories but also for industrial applications.

SUPPLEMENTARY INFORMATION

The online version contains supplementary material available at <https://doi.org/10.1208/s12249-022-02234-8>.

AUTHOR CONTRIBUTION

AP and JW contribute to the conceptualization and design of the work. The samples were prepared by JM. AP performed all of the experiments and data acquisition. Data was analyzed and visualized by AP and JW. The original draft was written by JW, while AP and JM helped with review and editing. All authors have read and agreed to the published version of the manuscript.

FUNDING

The work was part-financed by the Plenipotentiary of Poland to JINR, Dubna, Program “A study of the structure and molecular dynamics in crystalline and amorphous therapeutic compounds.”

DECLARATIONS

Conflict of Interest The authors declare no competing interests.

REFERENCES

- Kawabata Y, Wada K, Nakatani M, Yamada S, Onoue S. Formulation design for poorly water-soluble drugs based on biopharmaceutics classification system: basic approaches and practical applications. *Int J Pharm.* 2011;42:1–10.
- Renuka, Singh SK, Gulati M, Narang R. Stable amorphous binary systems of glipizide and atorvastatin powders with enhanced dissolution profiles: formulation and characterization. *Pharm Dev Technol.* 2017;22:13–25.
- Takagi T, Ramachandran C, Bermejo M, Yamashita S, Yu LX, Amidon GL. A provisional biopharmaceutical classification of the top 200 oral drug products in the United States, Great Britain, Spain, and Japan *Mol Pharm.* 2006;3:631–643.
- Löbenberg R, Amidon GL. Modern bioavailability, bioequivalence and biopharmaceutics classification system. New scientific approaches to international regulatory standards. *Eur J Pharm Biopharm.* 2000;50:3–12.
- Hancock BC, Parks M. What is the true solubility advantage for amorphous pharmaceuticals? *Pharm Res.* 2000;17:397–403.
- Liu B, Theil F, Lehmkemper K, Gessner D, Li Y, Lishaut H. Crystallization risk assessment of amorphous solid dispersions by physical shelf-life modeling: a practical approach. *Mol Pharm.* 2001;18:2428–37.
- Waring MJ, Arrowsmith J, Leach AR, Leeson PD, Mandrell S, Owen RM, Pairaudeau G, Pennie WD, Pickett SD, Wang J, Wallace O, Weir A. An analysis of the attrition of drug candidates from four major pharmaceutical companies. *Nat Rev Drug Discov.* 2015;14:475–86.
- Palpandi P, Bulusu R, Kommineni N, Khan W, Singh M. Amorphous solid dispersions: an update for preparation, characterization, mechanism on bioavailability, stability, regulatory considerations and marketed products. *Int J Pharm.* 2020;586:1195603.
- Schittny A, Huwyler J, Puchkov M. Mechanisms of increased bioavailability through amorphous solid dispersions: a review. *Drug Delivery.* 2020;27:110–27.
- Pandi P, Bulusu R, Kommineni N, Khan W, Singh M. Amorphous solid dispersions: an update for preparation, characterization, mechanism on bioavailability, stability, regulatory considerations and marketed products. *Int J Pharm.* 2020;586:119560.
- Huang S, Williams RO. Effects of the preparation process on the properties of amorphous solid dispersions. *AAPS PharmSciTech.* 2018;19:1971–84.
- Konno H, Taylor LS. Ability of different polymers to inhibit the crystallization of amorphous felodipine in the presence of moisture. *Pharm Res.* 2008;25:969–78.
- Taylor LS, Braun DE, Steed JW. Crystals and crystallization in drug delivery design. *Mol Pharm.* 2021;18:751–3.
- Rumondor ACF, Marsac PJ, Stanford LA. Taylor LS Phase behavior of poly(vinylpyrrolidone) containing amorphous solid dispersions in the presence of moisture. *Mol Pharm.* 2009;6:1492–505.
- Bikiaris D, Papageorgiou GZ, Stergiou A, Pavlidou E, Karavas E, Kanaze F, Georganakis M. Physicochemical studies on solid dispersions of poorly water-soluble drugs: evaluation of capabilities and limitations of thermal analysis techniques. *Thermochim Acta.* 2005;439:58–67.
- Wegiel LA, Mauer LJ, Edgar KJ, Taylor LS. Crystallization of amorphous solid dispersions of resveratrol during preparation and storage - impact of different polymers. *J Pharm Sci.* 2013;102:171–84.
- Wang X, Zhang L, Ma D, Tang X, Zhang Y, Yin T, Gou J, Wang Y, He H. Characterizing and exploring the differences in dissolution and stability between crystalline solid dispersion and amorphous solid dispersion. *AAPS PharmSciTech.* 2020;21:262.
- Chmiel K, Knapik-Kowalczyk J, Jurkiewicz K, Sawicki W, Jachowicz R, Paluch M. A new method to identify physically stable concentration of amorphous solid dispersions (I): case of flutamide + kollidon VA64. *Mol Pharm.* 2017;14:3370–80.
- Paudel A, Geppi M, Mooter G. Structural and dynamic properties of amorphous solid dispersions: the role of solid-state nuclear magnetic resonance spectroscopy and relaxometry. *J Pharm Sci.* 2014;103:2635–62.
- Mollica G, Geppi M, Pignatello R, Veracini CA. Molecular properties of flurbiprofen and its solid dispersions with Eudragit RL100 studied by high- and low-resolution solid-state nuclear magnetic resonance. *Pharm Res.* 2006;23:2129–40.
- Lu X, Huang C, Lowinger MB, Yang F, Xu W, Brown CW, Hesk D, Koynov A, Schenck L, Su Y. Molecular interactions in posaconazole amorphous solid dispersions from two-dimensional solid-state NMR spectroscopy. *Mol Pharm.* 2019;16:2579–89.
- Pham TN, Watson SA, Edwards AJ, Chavda M, Clawson JS, Strohmeier M, Vogt FG. Analysis of amorphous solid dispersions using 2D solid-state NMR and ^1H T_1 relaxation measurements. *Mol Pharm.* 2010;7:1667–91.
- Li M, Xu W, Su Y. Solid-state NMR spectroscopy in pharmaceutical sciences. *Trends Anal Chem.* 2021;135:116152.
- Aso Y, Yoshioka S, Miyazaki T, Kawanishi T, Tanaka K, Kitamura S, Takakura A, Hayashi T, Muranushi N. Miscibility of nifedipine and hydrophilic polymers as measured by ^1H -NMR spin-lattice relaxation. *Chem Pharm Bull.* 2007;55:1227–31.
- Tishmack PA, Bugay DE, Byrn SR. Solid-state nuclear magnetic resonance spectroscopy in pharmaceutical applications. *J Pharm Sci.* 2003;92:441–74.
- Geppi M, Borsacchi S, Carignani E. Study of disorder by solid-state NMR spectroscopy. In: *Disordered Pharmaceutical Materials*, M. Descamps (Ed.); 2016.
- Geppi M, Mollica G, Borsacchi S, Veracini CA. Solid-state NMR studies of pharmaceutical systems. *Appl Spectr Reviews* 2008;43:202–302
- Carignani E, Geppi LM, Combarieu Em Borsacchi S. Solid state NMR of the mixing degree between Ginkgo biloba extract and a soy-lecithin-phosphatidylserine in a composite prepared by the phytosome method. *Chem Africa.* 2020;3:717–25.
- Okada K, Hirai D, Kumada S, Kosugi A, Hayashi Y, Onuki Y. ^1H NMR relaxation study to evaluate the crystalline state of active pharmaceutical ingredients containing solid dosage forms using time domain NMR. *J Pharm Sci* 2019;108:451–456.
- Stueber D, Jehle S. Quantitative component analysis of solid mixtures by analyzing time domain ^1H and ^{19}F T_1 saturation recovery curves (qSRC). *J Pharm Sci* 2017;106:1828–1838.
- Chattoraj S, Bhugra C, Li ZJ, Sun C. Effect of heating rate and kinetic model selection on activation energy of nonisothermal crystallization of amorphous felodipine. *J Pharm Sci.* 2014;103:3950–7.
- Praveen K, Arthanareeswari M, Ravikiran A, Kamaraj P, Pavan KV. Kinetic studied on crystallization process of amorphous Vilazodone hydrochloride. *Int J Pharm Sci.* 2014;6:630–5.
- Crowley KJ, Zografí G. The effect of low concentrations of molecularly dispersed poly(vinylpyrrolidone) on indomethacin crystallization from the amorphous state. *Pharm Res.* 2003;20:1417–22.
- Zhu L, Jona J, Nagapudi K, Wu T. Fast surface crystallization of amorphous griseofulvin below T_g . *Pharm Res.* 2010;27:1558–67.
- Kestur US, Ivanovic I, Alonzo DE, Taylor LS. Influence of particle size on the crystallization kinetics of amorphous felodipine powders. *Powder Technol.* 2013;236:197–204.

36. Marsac PJ, Konno H, Taylor LS. A comparison of the physical stability of amorphous felodipine and nifedipine systems. *Pharm Res.* 2006;23:2306–16.
37. Marsac PJ, Konno H, Rumondor ACF, Taylor LS. Recrystallization of nifedipine and felodipine from amorphous molecular level solid dispersions containing poly(vinylpyrrolidone) and sorbed water. *Pharm Res.* 2008;25:647–56.
38. Zhu L, Wong L, Yu L. Surface-enhanced crystallization of amorphous nifedipine. *Mol Pharm.* 2008;5:921–6.
39. Kestur US, Taylor LS. Role of polymer chemistry in influencing crystal growth rates from amorphous felodipine. *Cryst Eng Comm.* 2010;12:2390–7.
40. Ricarte RG, Lodge TP, Hillmyer MA. Detection of pharmaceutical drug crystallites in solid dispersions by transmission electron microscopy. *Mol Pharm.* 2015;12:983–99.
41. Alonzo DE, Zhang GGZ, Zhou D, Gao Y, Taylor LS. Understanding the behavior of amorphous pharmaceutical systems during dissolution. *Pharm Res.* 2010;27:608–18.
42. Kaminska E, Tarnacka M, Włodarczyk P, Jurkiewicz K, Kolodziejczyk K, Dulski M, Haznar-Garbacz D, Hawelek L, Kaminski K, Włodarczyk A, Paluch M. Studying the impact of modified saccharides on the molecular dynamics and crystallization tendencies of model api nifedipine. *Mol Pharm.* 2015;12:3007–19.
43. Sibik J, Löbmann K, Rades T, Zeitler JA. Predicting crystallization of amorphous drugs with terahertz spectroscopy. *Mol Pharm.* 2015;12:3062–8.
44. Pajzderska A, Fojud Z, Jarek M, Wasicki J. NMR relaxometry In the investigation of the kinetics of the recrystallization of felodipine. *Powder Technol.* 2019;347:35–41.
45. Pajzderska A, Wasicki J. NMR relaxometry in a investigation of the kinetics of the recrystallization of a three-phase system. *Int J Pharm.* 2021;605:120800.
46. Rumondor ACF, Stanford LA, Taylor LS. Effects of polymer type and storage relative humidity on the kinetics of felodipine crystallization from amorphous solid dispersions. *Pharm Res.* 2009;26:2599–606.
47. Tang XC, Pikal MJ, Taylor LS. A spectroscopic investigation of hydrogen bond patterns in crystalline and amorphous phases in dihydropyridine calcium channel blockers. *Pharm Res.* 2002;19:477–83.
48. Pajzderska A, Drużbicki K, Gonzalez MA, Jencyk J, Mielcarek J, Wąsicki J. Diversity of methyl group dynamics in felodipine: a DFT supported NMR and neutron scattering study. *Cryst Eng Comm.* 2018;20:7371–85.
49. Pajzderska A, Jencyk J, Embs JP, Wasicki J. Exploring molecular reorientations in amorphous and recrystallized felodipine at the microscopic level. *RSC Adv.* 2020;10:37346–57.
50. Konno H, Taylor LS. Ability of different polymers to inhibit the crystallization of amorphous, felodipine in the presence of moisture. *Pharm Res.* 2008;25:969–78.
51. Rumondor ACF, Ivanisevic I, Bates S, Alonzo DE, Taylor LS. Evaluation of drug-polymer miscibility in amorphous solid dispersion systems. *Pharm Res.* 2009;26:2523–34.
52. Qi S, Belton P, Nollenberger K, Clayden N, Reading M, Craig DQM. Characterisation and prediction of phase separation in hot-melt extruded solid dispersions: a thermal, microscopic and NMR relaxometry study. *Pharm Res.* 2010;27:1869–83.
53. Ivanisevic I. Physical stability studies of miscible amorphous solid dispersions. *J Pharm Sci.* 2010;99:4005–12.
54. Luebbert C, Klanke C, Sadowski G. Investigating phase separation in amorphous solid dispersions via Raman mapping. *Int J Pharm.* 2017;535:245–52.
55. Luebbert C, Wessner M, Sadowski G. Mutual impact of phase separation/crystallization and water sorption in amorphous solid dispersions. *Mol Pharm.* 2018;15:669–78.
56. Sarpal K, Delaney S, Zhang GGZ, Munson EJ. Phase behavior of amorphous solid dispersions of felodipine: homogeneity and drug-polymer interactions. *Mol Pharm.* 2019;16:4836–51.
57. Ueda K, Okada H, Zhao Z, Higashi K, Moribe K. Application of solid-state ¹³C relaxation time to prediction of the recrystallization inhibition strength of polymers on amorphous felodipine at low polymer loading. *Int J Pharm.* 2020;581:119300.
58. Baghel S, Cathcart H, O'Reilly NJ. Polymeric amorphous solid dispersions: a review of amorphization, crystallization, stabilization, solid-state characterization, aqueous solubilization of biopharmaceutical classification system class II drugs. *J Pharm Sci.* 2016;105:2527–44.
59. Gordon M, Taylor LS. Ideal copolymers and the second-order transitions of synthetic rubbers. I. Non-crystalline copolymers. *J Appl Chem.* 1952;2:493–500.
60. Powles JG, Mansfield P. Double-pulse nuclear resonance transients in solids. *Phys Lett.* 1962;2:58–9.
61. Powles JG, Strange JH. Zero time resolution nuclear magnetic resonance transients in solids. *Proc Phys Soc.* 1963;82:6–15.
62. PeakFit-Jandel Scientific Software, San Rafael, CA
63. Schmidt-Rohr K, Spiess HW. London: Multidimensional solid-state N.M.R. and polymers Academic Press Limited; 1994.
64. Guo M. Solid-state high-resolution NMR studies on the miscibility of polymer blends. *Trends Polym Sci.* 1996;7:238–44.
65. Clauss J, Schmidt-Rohr K, Spiess HW. Determination of domain size in heterogeneous polymers by solid-state NMR. *Acta Polym.* 1993;44:1–17.
66. Spiegel S, Schmidt-Rohr K, Boeffel C, Spiess HW. ¹H spin diffusion coefficients of highly mobile polymers. *Polymer.* 1993;34:4566–9.
67. Qi S, Moffat JG, Yang Z. Early stage phase separation in pharmaceutical solid dispersion thin films under high humidity: improved spatial understanding using probe-based thermal and spectroscopic nanocharacterization methods. *Mol Pharm.* 2013;10:918–30.

Publisher's Note Springer Nature remains neutral with regard to jurisdictional claims in published maps and institutional affiliations.